

Energy & Environmental Science

Accepted Manuscript



This is an *Accepted Manuscript*, which has been through the Royal Society of Chemistry peer review process and has been accepted for publication.

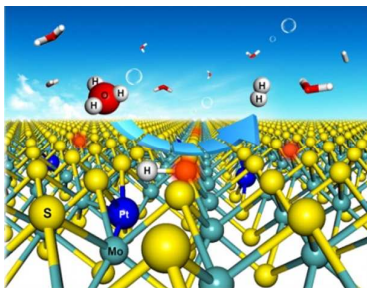
Accepted Manuscripts are published online shortly after acceptance, before technical editing, formatting and proof reading. Using this free service, authors can make their results available to the community, in citable form, before we publish the edited article. We will replace this *Accepted Manuscript* with the edited and formatted *Advance Article* as soon as it is available.

You can find more information about *Accepted Manuscripts* in the [Information for Authors](#).

Please note that technical editing may introduce minor changes to the text and/or graphics, which may alter content. The journal's standard [Terms & Conditions](#) and the [Ethical guidelines](#) still apply. In no event shall the Royal Society of Chemistry be held responsible for any errors or omissions in this *Accepted Manuscript* or any consequences arising from the use of any information it contains.

Entry for the Table of Contents

Doping single-atom metals into the matrix of MoS₂ can efficiently arouse the electrocatalytic hydrogen evolution activity of inert S atoms on the two-dimensional MoS₂ surface and meanwhile enhance the catalytic stability and anti-poison ability.



Arousing the electrocatalytic hydrogen evolution activity of inert two-dimensional MoS₂ surface via single-atom metal doping

Jiao Deng^{†1}, Haobo Li^{†1}, Jianping Xiao¹, Yunchuan Tu¹, Dehui Deng^{*1}, Huaixin Yang², Huanfang Tian², Jianqi Li², Pengju Ren¹, Xinhe Bao^{*1}

¹State Key Laboratory of Catalysis, *i*ChEM, Dalian Institute of Chemical Physics, Chinese Academy of Sciences, Dalian, 116023, China.

²Beijing National Laboratory for Condensed Matter Physics, Institute of Physics, Chinese Academy of Sciences, Beijing 100190, China.

[†]These authors have contributed equally.

*E-mail: dhdeng@dicp.ac.cn; xhbao@dicp.ac.cn; Fax: +86-411-84379128; Tel: +86-411-84686637.

Abstract

Electrocatalytic splitting of water is one of the most efficient technologies for hydrogen production, and two-dimensional (2D) MoS₂ has been considered as a potential alternative to Pt-based catalysts in hydrogen evolution reaction (HER). However, the catalytic activity of 2D MoS₂ is always contributed from its edge sites, leaving a large number of in-plane domains useless. Herein, we for the first time demonstrated that the catalytic activity of in-plane S atoms of MoS₂ can be aroused via single-atom metal doping in HER. The single-Pt atoms doped few-layer MoS₂ nanosheets (Pt-MoS₂) in experiments showed a significantly enhanced HER activity compared with pure MoS₂, which originates from the tuned adsorption behavior of H atoms on the in-plane S sites neighboring to doped Pt atoms according to the density functional theory (DFT) calculations. Furthermore, the HER activity of a number of transition metals doped MoS₂ was screened by virtue of DFT calculations and presented a volcano curve along the adsorption free energy of H atoms ($\Delta G_{\text{H}}^{\circ}$), which was further confirmed in experiment by using non-precious metals such as Co and Ni atoms doped 2D MoS₂ as the catalysts.

Introduction

Two-dimensional (2D) MoS₂ crystal with intriguing physical and chemical properties has attracted increasing attention in numerous research fields during the past few years¹⁻⁶. Especially, it possesses a variety of advantages in structural and electronic properties, which can boost its potential applications in varied catalytic processes such as hydrodesulfurization^{7, 8}, catalytic hydrogenation^{9, 10}, syngas conversion to alcohol^{11, 12}, and water splitting¹³⁻¹⁸. At present, there is a consensus that the active centers of MoS₂ correspond to the coordinatively unsaturated S atoms along its edges^{7, 9, 11, 15, 19}, while the perfect in-plane domain of MoS₂ is always inert. Thus, it is of great interests to explore the strategies to stimulate the catalytic activity of inert in-plane atoms of 2D MoS₂, but it still remains as a great challenge due to the lack of efficient experimental techniques and theoretical understanding. Inspired by the cases of heteroatoms doped 2D graphene²⁰⁻²², in which the electronic properties of the carbon atoms neighboring to the doped heteroatoms can be significantly modulated and thereby the catalytic activity of in-plane carbon atoms would be altered, the introduction of doped atoms into the 2D MoS₂ in-plane area may achieve the goal. However, to the best of our knowledge, there is no systematic report about the correlations between dopants and the catalytic activity of in-plane atoms of 2D MoS₂. Therefore, by focusing on the electrocatalytic hydrogen evolution reaction (HER), a highly important energy-conversion process for hydrogen production^{23, 24}, we for the first time observed the enhanced catalytic activity via single-atom metal doping, attributed to the stimulating activity of in-plane S atoms of 2D MoS₂.

We firstly successfully introduced single-Pt atoms into the in-plane domain of few-layer MoS₂ nanosheets (Pt-MoS₂) via a directly chemical synthesis method. It was found that a distinct enhancement of HER activity of Pt-MoS₂ was achieved compared with pure 2D MoS₂, as well as high stability in acidic medium. The density functional theory (DFT) calculations indicated that the doped Pt atoms can tune the adsorption behavior of H atoms on the neighboring S sites and consequently the HER activity, which originates from the novel electronic states of Pt-MoS₂. Furthermore,

the HER activity of a number of transition metals doped MoS₂ was screened by virtue of DFT calculations, which presents a volcano curve along the adsorption free energy of H atoms ($\Delta G_{\text{H}}^{\circ}$). Finally, the non-precious-metals Co and Ni doped MoS₂ were investigated as the HER catalysts, further validating the volcano plot. The findings in this work illustrate the viability to arouse the catalytic activity of inert in-plane atoms of MoS₂ via single-atom metal doping.

Experimental section

Materials synthesis.

The Pt-MoS₂ was synthesized through a one-pot chemical method. Firstly, 900 mg (NH₄)₆Mo₇O₂₄·4H₂O and 0.442 mL 0.19 mol L⁻¹ H₂PtCl₆ (aq.) were dissolved in 20 mL deionized water to form a homogeneous solution. Then, the solution and 10 mL CS₂ were transferred into a 40 mL stainless steel autoclave under Ar and maintained at 400 °C for 4 h. The final product was treated with saturated NaOH (aq.) under stirring at 60 °C for 3 h, followed by washing with water and absolute ethanol for several times and drying at 100 °C. For comparison, the pure few-layer MoS₂ (FL-MoS₂) was synthesized by using 900 mg (NH₄)₆Mo₇O₂₄·4H₂O dissolved in 20 mL deionized water and 10 mL CS₂ conducted within the same process as the Pt-MoS₂. The Pt/MoS₂ was prepared by wet-impregnating 0.092 mL 0.19 mol L⁻¹ H₂PtCl₆ (aq.) onto 200 mg pure FL-MoS₂ following with a reduction process by H₂ at 250 °C for 1h. The Co-MoS₂ and Ni-MoS₂ were synthesized by using 900 mg (NH₄)₆Mo₇O₂₄·4H₂O and 0.085 g Co(NO₃)₂·6H₂O or 0.084 g Ni(NO₃)₂·6H₂O dissolved in 20 mL deionized water and 10 mL CS₂ conducted within the same process as the Pt-MoS₂.

Materials characterization.

Transmission electron microscopy (TEM) was carried out on a FEI Tecnai F30 microscope and a G² microscope operated at an accelerating voltage of 300 and 120 kV, respectively. High angle annular dark field-scanning transmission electron microscopy (HAADF-STEM) was performed on JEOL ARM200F equipped with

double aberration correctors and cold field emission gun which was operated at 80 kV. Energy dispersive X-ray (EDX) mapping was carried out on a spherical aberration corrected transmission electron microscope (FEI Titan G2 80-200) which was operated at 200 kV. Extended X-ray absorption fine structure (EXAFS) and X-ray absorption near-edge spectra (XANES) were measured at the BL14W1 beamline of the Shanghai Synchrotron Radiation Facility (SSRF). X-ray diffraction (XRD) measurements were conducted on a Rigaku D/MAX 2500 diffractometer with Cu K α radiation ($\lambda=1.5418 \text{ \AA}$) at 40 kV and 200 mA. Raman spectroscopy was performed on a Jobin Yvon LabRAM HR 800 instrument with a 532 nm excitation laser at a power of 0.7 mW. Inductively coupled plasma optical emission spectroscopy (ICP-OES) was carried out in Perkin-Elmer Optima 7300DV.

Electrochemical measurements.

HER polarization curve tests were conducted on a 2273 potentiostat/galvanostat with a three-electrode electrochemical cell equipped with a gas flow controlling system. Graphite rod was used as the counter electrode and Ag/AgCl (saturated KCl-filled) as the reference electrode. A glassy carbon rotating disk electrode with a diameter of 5 mm covered by a thin catalyst film was used as the working electrode. Typically, 3.3 mg catalyst (for bulk MoS₂, FL-MoS₂ and Pt-MoS₂) with 1.7 mg carbon black (Vulcan XC 72) was suspended in 2 mL ethanol with 50 μL Nafion solution (5 wt.%, Du Pont) to form a homogeneous ink assisted by ultrasound. Then 125 μL of the ink was spread onto the surface of glassy carbon by a micropipette and dried under room temperature. The final Pt loading of Pt-MoS₂ on work electrode is 0.018 mg/cm². For 40% Pt/C, 5 mg catalyst was suspended in 2 mL ethanol with 50 μL Nafion solution and followed with the same process as Pt-MoS₂, which giving a final Pt loading of 0.64 mg/cm² on work electrode. HER tests were conducted in a N₂ saturated 0.1 M H₂SO₄ electrolyte at 25 °C. The potential range was from 0 to -1.0 V (vs. Ag/AgCl) and the scan rate was 2 mV s⁻¹. Before measurements, the samples were repeatedly swept from -0.4 to 0.3 V (vs. Ag/AgCl) in the electrolyte until a steady voltammogram curve was obtained. All the final potentials have been calibrated with respect to a reversible hydrogen electrode (RHE).

DFT calculations.

Theoretical calculations were performed using Vienna *ab initio* simulation packages (VASP)²⁵ with the projector-augmented wave (PAW) method²⁶. All calculations were based on the same generalized gradient approximation method with Perdew-Burke-Ernzerhof (PBE)²⁷ functional for the exchange-correlation term. The plane wave cutoff was set to 400 eV. The Brillouin zone was sampled by a $6 \times 6 \times 1$ k -point grid for the calculations on density of states (DOS) and a $3 \times 3 \times 1$ Monkhorst-Pack²⁸ k -point sampling for structural optimizations. The convergence of energy and forces were set to 1×10^{-5} eV and 0.05 eV/Å, respectively. The reaction barriers were calculated using the nudged elastic band (NEB) method²⁹ with van der Waals (vdW) corrections in the form of C^6/R^6 pair potentials (PBE-D)³⁰. C^6 for Mo, S, Pt, O and H is chosen to be 24.67, 5.57, 24.67, 0.70, 0.14 J nm⁶ mol⁻¹; and the vdW radius, R^0 , is set as 1.639, 1.683, 1.75, 1.342, 1.001 Å, respectively.

Results and discussion

The single-Pt atoms doped few-layer MoS₂ nanosheets (Pt-MoS₂) was prepared via a one-pot chemical reaction by using (NH₄)₆Mo₇O₂₄, H₂PtCl₆ and CS₂ as precursors (see the experimental section for details). The transmission electron microscopy (TEM) image in Fig. 1a shows that Pt-MoS₂ consist of flower-like 2D nanosheets with a layer distance of 0.62 nm, corresponding to the (002) plane of MoS₂. According to the TEM image, no nanoparticles or large clusters of Pt were observed, consistent with the energy dispersive X-ray (EDX) mapping (Fig. 1g-j) showing the homogeneous distribution of Mo, S and Pt atoms over the entire nanosheets and the X-ray diffraction (XRD) patterns showing no Pt-containing crystal phases (Fig. S1). Furthermore, sub-angstrom resolution high angle annular dark field-scanning transmission electron microscopy (HAADF-STEM) images clearly exhibits single-Pt atoms (brighter white dots in Fig. 1b-c) uniformly disperse in the 2D MoS₂ plane and the magnified domain from Fig. 1c reveals that single-Pt atoms exactly occupy the positions of the Mo atoms (Fig. 1d). In addition, the extended

X-ray absorption fine structure (EXAFS) spectra show there is no Pt-Pt bond in Pt-MoS₂ (Fig. 1e), further confirming that no Pt particles or clusters existed in Pt-MoS₂. Instead, it appears an obvious peak at about 2.2 Å, corresponding to the Pt-S bond according to the literature^{31,32}. X-ray absorption near-edge structure (XANES) spectra also showed that the intensity of Pt L₃-edge in Pt-MoS₂ is obviously higher than that in Pt foil and 40% Pt/C (Fig. 1f), indicating that the Pt atoms have positive charges which should be attributed to Pt-S bonds leading the electron transfer from Pt to S in the MoS₂ network. These results demonstrate that single-Pt atoms have been successfully doped into the 2D MoS₂ network via the substitution of Mo sites.

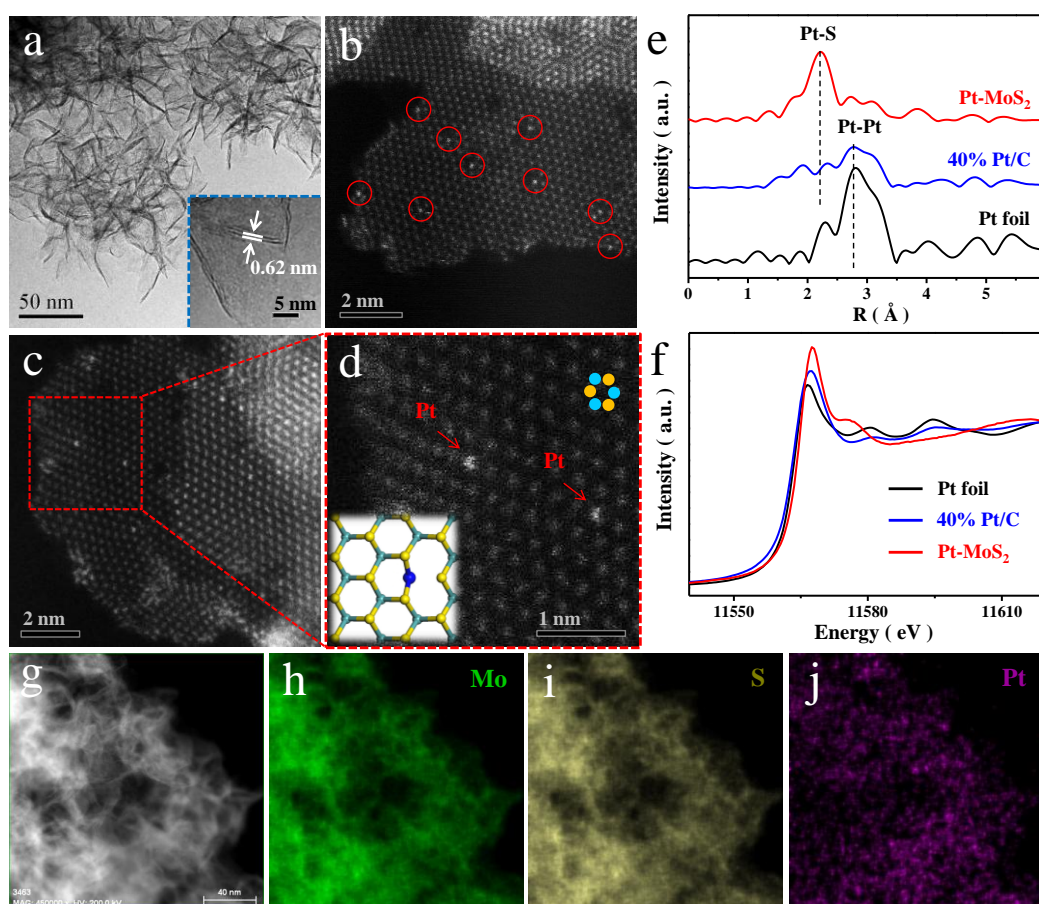


Fig. 1 (a) TEM image of Pt-MoS₂ with the inset showing a typical MoS₂ layer distance of 0.62 nm. (b-c) HAADF-STEM images of Pt-MoS₂ showing that the single-Pt atoms (marked by red circles in figure b) uniformly disperse in the 2D MoS₂ plane. (d) Magnified domain with red dashed rectangle in figure c showing a honeycomb arrangement of MoS₂ and the single-Pt atoms occupy exactly the

positions of the Mo atoms (marked by red arrows). The bottom inset shows the simulated configuration of Pt-MoS₂. The green, yellow and blue balls represent Mo, S and Pt, respectively. (e) The k²-weighted EXAFS spectra of Pt-MoS₂ in comparison to Pt foil and commercial 40% Pt/C. (f) The normalized Pt L₃-edge XANES spectra of Pt-MoS₂ in comparison to Pt foil and commercial 40% Pt/C. (g-j) HAADF-STEM image and corresponding EDX mapping images of Pt-MoS₂ showing the homogeneous distribution of Mo, S and Pt elements within the 2D nanosheets: (h) Mo, (i) S and (j) Pt elements' imaging, respectively.

2D MoS₂ has been widely studied in the electrocatalytic hydrogen evolution reaction (HER), but due to the active centers only originate from its edge sites leaving a large number of in-plane domains useless¹⁴⁻¹⁶, the activity of pure MoS₂ is still not satisfying. Therefore, in order to achieve an enhanced catalytic activity of in-plane MoS₂, we investigate the effect of single-Pt atom dopants on HER. A typical three-electrode setup in 0.1 M H₂SO₄ electrolyte was adopted to carry out the HER measurements. As shown in Fig. 2a, both blank glassy carbon (GC) electrode and bulk MoS₂ exhibited poor HER activities, and the pure few-layer MoS₂ nanosheets (FL-MoS₂) without Pt atoms doping showed a higher activity but is still much inferior to 40% Pt/C catalyst. In contrast, after the Pt atoms doping, Pt-MoS₂ showed a distinctly enhanced activity by reducing the overpotential of about 60 mV relative to FL-MoS₂ at current density of 10 mA cm⁻². Furthermore, the Pt-MoS₂ catalyst also exhibited a very stable performance within the accelerated degradation measurements by 5000 cyclic voltammetric (CV) sweeps (Fig. 2c). As shown in Fig. 2d, from the potential values recorded at the current density of 1 mA cm⁻², 5 mA cm⁻² and 10 mA cm⁻² with different CV sweeps, one can see that Pt-MoS₂ showed only a slight degradation in the activity. Considering the content of Pt in Pt-MoS₂ is only 1.7 wt.% (measured by ICP-OES) and no obvious difference was observed in the XRD patterns (Fig. S1), Raman spectra (Fig. S2) and TEM images (Fig. S3) of these samples before

and after Pt atoms doping, the HER activity modulation was not led by the structural variations, but attributed to the modulation of the electronic properties of Pt-MoS₂.

Tafel slope was used to reveal the inherent reaction process of HER. As shown in Fig. 2b, the value of Pt-MoS₂ (96 mV/dec) is quite different from that of a Pt/C electrocatalyst (32 mV/dec), indicating that the mechanism should deviate from that on Pt. Instead, it is more similar to that on FL-MoS₂ (98 mV/dec), suggesting the HER on Pt-MoS₂ resembles the reaction mechanism on pristine MoS₂, i.e., following a Volmer-Heyrovsky mechanism³³⁻³⁵. In other words, the active sites of HER should also originate from the S atoms instead of the Pt atoms in the Pt-MoS₂ sample.

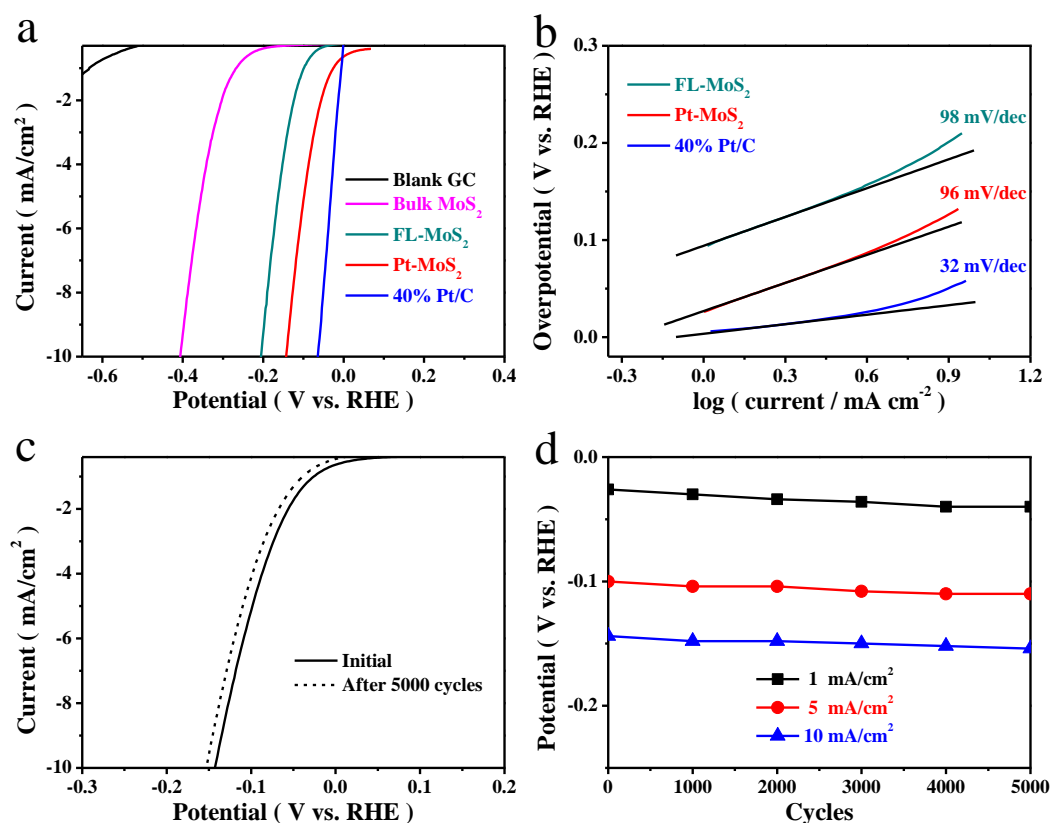


Fig. 2 (a) HER polarization curves for Pt-MoS₂ in comparison with blank GC electrode, bulk MoS₂, FL-MoS₂, and 40% Pt/C. (b) Tafel plots for FL-MoS₂, Pt-MoS₂ and 40% Pt/C, respectively. (c) Durability measurement of Pt-MoS₂. The polarization curves were recorded initially and after 5000 CV sweeps between -0.13 V and +0.57 V (vs. RHE) at 100 mV s⁻¹. (d) Potential values recorded initially and after every 1000 CV sweeps from the polarization curves of durability measurement for Pt-MoS₂ at 1

mA cm⁻², 5 mA cm⁻² and 10 mA cm⁻², respectively. All the HER measurements were conducted in a N₂ saturated 0.1 M H₂SO₄ electrolyte at 25 °C.

Density functional theory (DFT) calculations were carried out to gain the nature of the catalytic process in Pt-MoS₂. According to the theoretical optimization results of the different single-atom Pt doped MoS₂ configurations by adopting a periodically repeated single layer MoS₂ (a trilayer unit of S-Mo-S as a single layer³⁶) crystal model, the most stable structure of different doping configurations is that directly replacing in-plane Mo atoms with doped Pt atoms, resulting in a substitutional doping structure (see Fig. S4 for details).

The elementary reaction steps of HER can be briefly described by a three-state process consisting of initial state (H⁺), adsorbed intermediate state (H*), and terminal product (1/2 H₂). It has been demonstrated that the adsorption free energy of H* ($\Delta G_{\text{H}^*}^{\circ}$) is a widely accepted descriptor of HER activity on a broad range of possible catalytic materials³⁷⁻³⁹. A good catalyst for HER should have a moderate $\Delta G_{\text{H}^*}^{\circ}$ (~0) to compromise the reaction barriers in the adsorption and desorption steps³⁷. Therefore, DFT calculations were conducted by adopting the above optimized configurations to examine the $\Delta G_{\text{H}^*}^{\circ}$ on a variety of adsorption sites including the Pt dopants, different S and Mo sites. It was found that only S atoms neighboring to the doped Pt are the prior adsorption sites (see Fig. S5). Most importantly, the $\Delta G_{\text{H}^*}^{\circ}$ on the in-plane S of Pt-doped MoS₂ is around 0 eV, while the $\Delta G_{\text{H}^*}^{\circ}$ on the edge S of a pure MoS₂ is about 0.1 eV which is consistent with the report in the literature³⁶. These calculated results indicate that the in-plane S atoms in the presence of Pt dopants can possess an even higher HER activity compared with the edge S atoms and thereby the introduction of Pt in MoS₂ can significantly enhance the HER activity, confirming the experimental results.

DFT calculations were further carried out to understand the electronic properties and chemical origins of HER activity on Pt-MoS₂. As shown in Fig. 3a, the calculated total density of states (DOS) showed there is a significant band gap in pure MoS₂,

while the position of the valence band moves downward and some hybridized electronic states occur nearby the Fermi level in Pt-MoS₂. When one H atom is absorbed on the S atom neighboring to the doped Pt atom of Pt-MoS₂ (as shown in Fig. 4 with the red dashed circle), a part of electronic states are saturated and disappeared above the Fermi level. The corresponding change could also be observed in the projected DOS of S atoms in the Pt-MoS₂, where the electronic states of in-plane S sites below the Fermi level increase significantly, which is quite comparable with that of the edge S atoms of a pure MoS₂ (Fig. 3a). The increased electronic states around the Fermi level can be attributed to the introduction of doped Pt atoms, thus resulting in the enhanced H adsorption ability of in-plane S atoms of Pt-MoS₂ and thereby the HER activity.

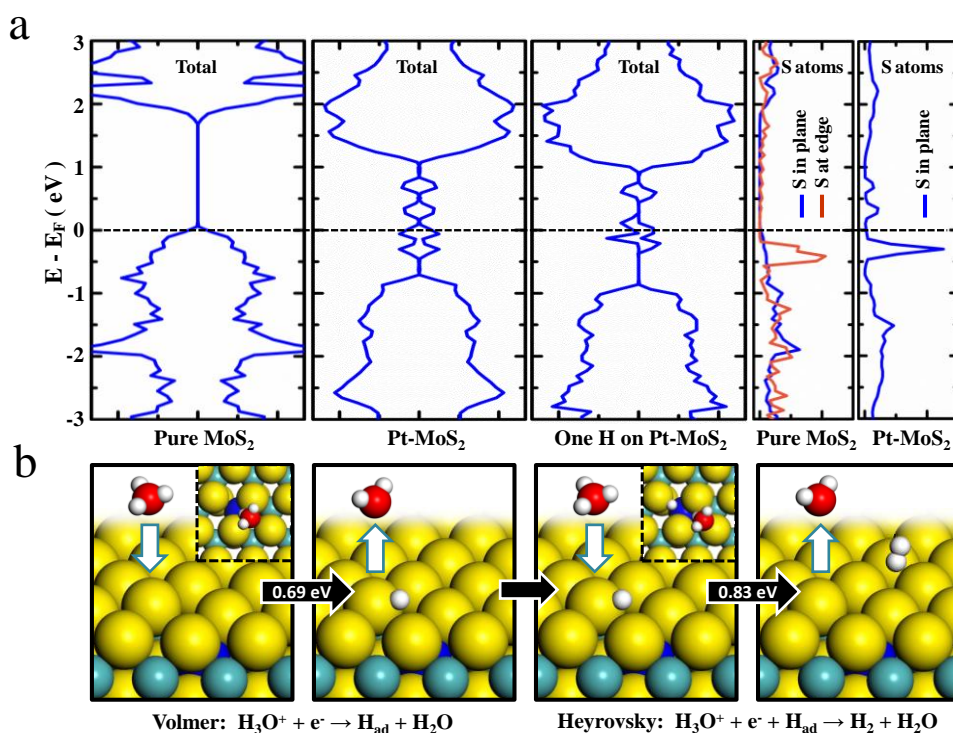


Fig. 3 (a) Total DOS for the pure MoS₂, Pt-MoS₂, one H absorbed on Pt-MoS₂, and projected DOS of in-plane and edge S atoms from pure MoS₂ and Pt-MoS₂, respectively. The position of the Fermi level is as shown in dashed lines. (b) HER process on a Pt-MoS₂ catalyst. The top views are shown in the insets. The reaction barriers are shown in the black arrows. The green, yellow, blue, red and white balls represent Mo, S, Pt, O and H atoms, respectively.

The reaction pathway was also investigated to understand the HER reaction mechanism on Pt-MoS₂. As shown in Fig. 3b, the unsaturated S atom is favorable to absorb one H atom with a barrier of about 0.69 eV. Then the absorbed H atom reacts with a hydrated proton, meanwhile receiving an electron to produce one H₂ molecule with a moderate energy barrier of 0.83 eV (Fig. 3b), following the Volmer-Heyrovsky mechanism, consistent with the analysis of the measured Tafel slope in Fig. 2b.

In order to further address the advantage of 2D MoS₂ with Pt atoms doping case (Pt-MoS₂), we compared its performance with that of the Pt supported on 2D MoS₂ (Pt/MoS₂) (Pt loading of 1.6 wt.% by ICP-OES, see the experimental section for the preparation process). The HER measurements showed that both samples of Pt-MoS₂ and Pt/MoS₂ owned a similar HER activity (Fig. S6), which agrees well with the results of DFT calculations with a similar $\Delta G_{\text{H}}^{\circ}$ on the unsaturated S atom of doped case and on the Pt atom of supported case (Fig. S7). However, Pt-MoS₂ possessed significantly higher durability than Pt/MoS₂ (Fig. S6), also consistent with the DFT calculations exhibiting the doping-configurations are more stable than the supported-configurations (Fig. S4). The durability of Pt-MoS₂ and Pt/MoS₂ was further investigated by the measurements with regard to the resistance of poisoning by methanol. The poisoning resistance ability of Pt-MoS₂ resembles that of FL-MoS₂ catalyst in the same condition (Fig. S8). In contrast, the activity of Pt/MoS₂ will drop quickly after adding methanol because the exposed Pt atoms are easily poisoned by methanol. These results demonstrate that the single-Pt atoms doping MoS₂ has a superior catalytic stability and poisoning resistance compared with Pt/MoS₂, because the Pt atoms in the doped case can not contact the reaction medium and reactants compared with the supported case.

In view of the successfully arousing catalytic activity of inert 2D MoS₂ surface via single-atom Pt doping, the HER activity of a number of single-metal atoms doped MoS₂ were investigated by virtue of DFT calculations. It was found that when metal atoms substitute the Mo atoms in the MoS₂ matrix, some metal atoms (e.g. V, Ti, Fe,

Mn, Cr etc.) prefer to remain in the middle to bond with six S atoms, while other atoms (e.g. Pt, Ag, Pd, Co, Ni etc.) tend to shift toward one side and be bonded with only four S atoms, leaving the other two S atoms unsaturated (see the inserted configuration graphs in Fig. 4). Such structural difference could cause distinctly different adsorption behavior of H atoms and thereby different HER activity resulting in the relation between currents ($\log(i_0)$) and $\Delta G_{\text{H}}^{\circ}$ presents a volcano curve (i_0 represents the exchange current density, Fig. 4), in which the metals on the left side tend to bind with four S atoms, while the others on the right side prefer to bind with six S atoms. As shown in Fig. 4, the Ni and Cu doped MoS_2 on the left side of volcano plot have relatively lower activity owing to the overly strong adsorption of H^* with the unsaturated S atoms neighboring to the dopants, whereas almost all doped MoS_2 on the right side can be anticipated to possess low activity due to their weak binding ability with H. Coincidentally, the Pt doped MoS_2 was on the top of the volcano plot, confirming the high HER activity of Pt- MoS_2 catalyst.

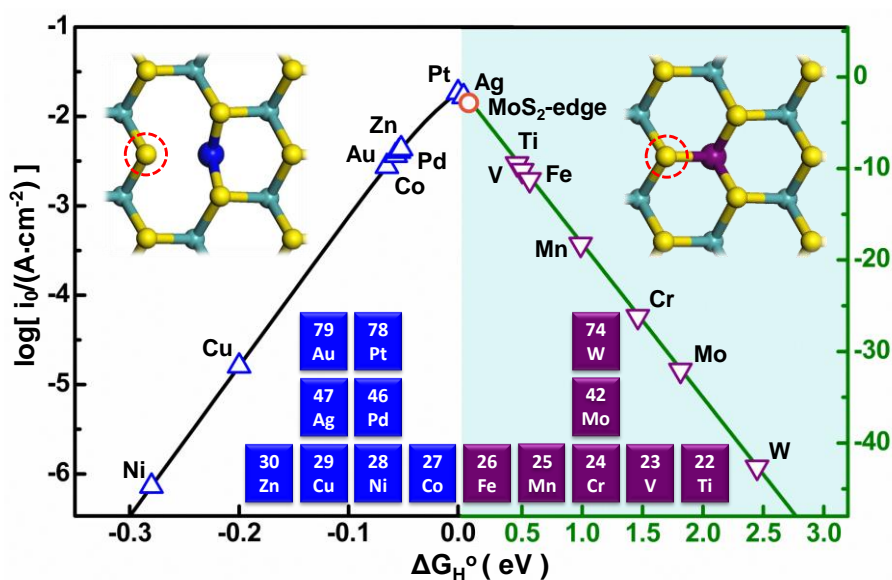


Fig. 4 The relation between currents ($\log(i_0)$) and $\Delta G_{\text{H}}^{\circ}$ presents a volcano curve. The left and right sides of the volcano plot adopt two sets of scales for better visibility. The inserted graphs point to different configurations of doped MoS_2 as coordinated with four (left) and six (right) S atoms. The adsorption sites for H atoms are marked by the red dashed circles. The studied metal atoms are located in the Periodic Table as shown

by the inset at the bottom. Green balls: Mo, yellow balls: S, blue and purple balls: doped metal atoms.

As predicted in the volcano plot for varied single-atom metals doped MoS₂ (Fig. 4), the non-precious metal dopants such as Co and Ni, could also be good candidates to tune the catalytic activity of MoS₂. Therefore, the Co (1.7 wt.% by ICP-OES) doped MoS₂ (Co-MoS₂) and the Ni (1.7 wt.% by ICP-OES) doped MoS₂ (Ni-MoS₂) were prepared following the same synthetic process as the Pt-MoS₂ (see experimental details in the experimental section). As shown in Fig. 5, Co-MoS₂ also exhibited an obviously enhanced HER activity by reducing the overpotential of about 20 mV relative to FL-MoS₂ at current density of 10 mA cm⁻² (Fig. 5a). Furthermore, the trend of HER activity in these doping cases is Pt > Co > Ni, which is in good agreement with the above calculated volcano plot. The non-precious metal atoms doped 2D MoS₂ also possess a high HER stability, e.g. the activity of Co-MoS₂ did not obviously decrease after 5000 CV sweeps (Fig. 5b).

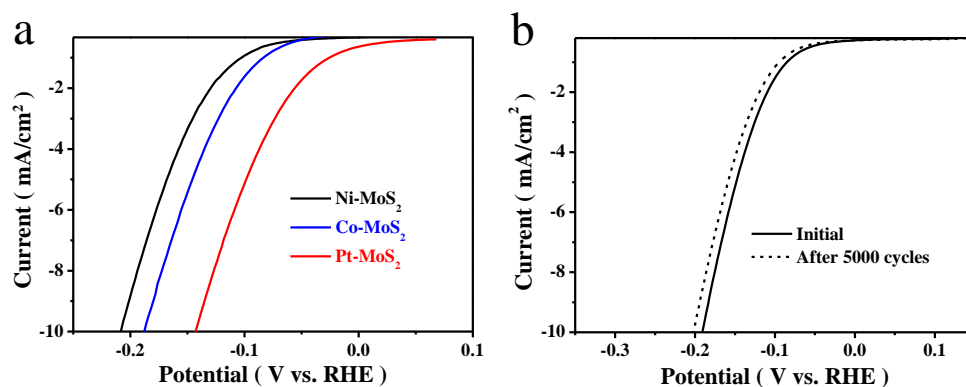


Fig. 5 (a) HER polarization curves for Ni-MoS₂, Co-MoS₂ and Pt-MoS₂, respectively. (b) Durability measurement of Co-MoS₂. The polarization curves were recorded initially and after 5000 CV sweeps between -0.13 V and +0.57 V (vs. RHE) at 100 mV s⁻¹. All the HER measurements were conducted in a N₂ saturated 0.1 M H₂SO₄ electrolyte at 25 °C.

Conclusion

In summary, we demonstrated that the catalytic activity of inert 2D MoS₂ surface can be efficiently aroused via single-metal atoms doping. Firstly, it was found from experiments that single-Pt atoms doped few-layer MoS₂ nanosheets (Pt-MoS₂) possess a significantly enhanced HER performance compared with that of pure 2D MoS₂, and also a more superior catalytic stability and poisoning resistance than Pt directly supported on 2D MoS₂. Then, the DFT calculations revealed that the doped Pt atoms can tune the adsorption behavior of H atoms on their neighboring S atoms and consequently the HER activity, which originates from the novel electronic states of Pt-MoS₂. The DFT calculations also revealed that the HER on Pt-MoS₂ follows a Volmer-Heyrovsky mechanism, which is consistent with our current experimental results. Finally, a range of metal atoms has been screened by virtue of DFT calculations resulting in the modulated ability of varied metal atoms presents as a volcano plot, and the HER measurements of Co and Ni doped MoS₂ in experiments further confirmed the volcano plot. The findings in the present work pave a rational pathway to arouse the activity of inert 2D MoS₂ surface in HER and also other energy-related catalytic processes with a high stability and anti-poison ability.

Acknowledgements

We gratefully acknowledge the financial support from the National Natural Science Foundation of China (No. 21321002 and 21303191), the strategic Priority Research Program of the Chinese Academy of Sciences (No. XDA09030100) and China Postdoctoral Science Foundation (No. 2014M551131), and the assistance from BL14W1 beamline of Shanghai Synchrotron Radiation Facilities (SSRF) for the EXAFS and XANES measurements. We thank Prof. Ze Zhang, Prof. Yong Wang and Mr. Wentao Yuan for help in EDX mapping characterization. We also acknowledge the computational resources from Shanghai Supercomputer Center (SSC).

References

1. M. S. Xu, T. Liang, M. M. Shi and H. Z. Chen, *Chem. Rev.*, 2013, **113**, 3766-3798.

2. Q. H. Wang, K. Kalantar-Zadeh, A. Kis, J. N. Coleman and M. S. Strano, *Nat. Nanotechnol.*, 2012, **7**, 699-712.
3. X. F. Liu, T. Xu, X. Wu, Z. H. Zhang, J. Yu, H. Qiu, J. H. Hong, C. H. Jin, J. X. Li, X. R. Wang, L. T. Sun and W. L. Guo, *Nat. Commun.*, 2013, **4**, 1776-1781.
4. K. S. Novoselov, D. Jiang, F. Schedin, T. J. Booth, V. V. Khotkevich, S. V. Morozov and A. K. Geim, *Proc. Natl. Acad. Sci. USA*, 2005, **102**, 10451-10453.
5. C. H. Lee, G. H. Lee, A. M. Zande, W. C. Chen, Y. L. Li, M. Y. Han, X. Cui, G. Arefe, C. Nuckolls, T. F. Heinz, J. Guo, J. Hone and P. Kim, *Nat. Nanotechnol.*, 2014, **9**, 676-681.
6. D. Merki and X. L. Hu, *Energy Environ. Sci.*, 2011, **4**, 3878-3888.
7. P. G. Moses, B. Hinnemann, H. Topsoe and J. K. Nørskov, *J. Catal.*, 2007, **248**, 188-203.
8. P. G. Moses, L. C. Grabow, E. M. Fernandez, B. Hinnemann, H. Topsoe, K. G. Knudsen and J. K. Nørskov, *Catal. Lett.*, 2014, **144**, 1425-1432.
9. A. Wambecke, L. Jalowiecki, S. Kasztelan, J. Grimblot and J. P. Bonnelle, *J. Catal.*, 1988, **109**, 320-328.
10. M. Huang and K. Cho, *J. Phys. Chem. C*, 2009, **113**, 5238-5243.
11. S. Zaman and K. J. Smith, *Catal. Rev.*, 2012, **54**, 41-132.
12. V. P. Santos, B. van der Linden, A. Chojecki, G. Budroni, S. Corthals, H. Shibata, G. R. Meima, F. Kapteijn, M. Makkee and J. Gascon, *ACS Catal.*, 2013, **3**, 1634-1637.
13. A. B. Laursen, S. Kegnaes, S. Dahl and I. Chorkendorff, *Energy Environ. Sci.*, 2012, **5**, 5577-5591.
14. B. Hinnemann, P. G. Moses, J. Bonde, K. P. Jørgensen, J. H. Nielsen, S. Horch, I. Chorkendorff and J. K. Nørskov, *J. Am. Chem. Soc.*, 2005, **127**, 5308-5309.
15. T. F. Jaramillo, K. P. Jørgensen, J. Bonde, J. H. Nielsen, S. Horch and I. Chorkendorff, *Science*, 2007, **317**, 100-102.
16. Y. G. Li, H. L. Wang, L. M. Xie, Y. Y. Liang, G. S. Hong and H. J. Dai, *J. Am. Chem. Soc.*, 2011, **133**, 7296-7299.
17. X. Huang, Z. Y. Zeng, S. Y. Bao, M. F. Wang, X. Y. Qi, Z. X. Fan and H. Zhang, *Nat. Commun.*, 2013, **4**, 1444-1451.
18. J. Deng, W. T. Yuan, P. J. Ren, Y. Wang, D. H. Deng, Z. Zhang and X. H. Bao, *RSC Adv.*, 2014, **4**, 34733-34738.
19. M. V. Bollinger, J. V. Lauritsen, K. W. Jacobsen, J. K. Nørskov, S. Helveg and F. Besenbacher, *Phys. Rev. Lett.*, 2001, **87**, 196803.
20. X. W. Wang, G. Z. Sun, P. Routh, D. H. Kim, W. Huang and P. Chen, *Chem. Soc. Rev.*, 2014, **43**, 7067-7098.
21. D. H. Deng, X. L. Pan, L. A. Yu, Y. Cui, Y. P. Jiang, J. Qi, W. X. Li, Q. A. Fu, X. C. Ma, Q. K. Xue, G. Q. Sun and X. H. Bao, *Chem. Mater.*, 2011, **23**, 1188-1193.
22. L. M. Zhang, J. W. Yu, M. M. Yang, Q. Xie, H. L. Peng and Z. F. Liu, *Nat. Commun.*, 2013, **4**, 1443-1449.
23. M. S. Dresselhaus and I. L. Thomas, *Nature*, 2001, **414**, 332-337.
24. C. C. L. McCrory, S. Jung, I. M. Ferrer, S. M. Chatman, J. C. Peters and T. F. Jaramillo, *J. Am. Chem. Soc.*, 2015, DOI: 10.1021/ja510442p.
25. G. Kresse and J. Furthmüller, *Phys. Rev. B*, 1996, **54**, 11169-11186.
26. P. E. Blochl, *Phys. Rev. B*, 1994, **50**, 17953-17979.
27. J. P. Perdew, K. Burke and M. Ernzerhof, *Phys. Rev. Lett.*, 1996, **77**, 3865-3868.

28. H. J. Monkhorst and J. D. Pack, *Phys. Rev. B*, 1976, **13**, 5188-5192.
29. G. Henkelman and H. Jonsson, *J. Chem. Phys.*, 2000, **113**, 9978-9985.
30. S. Grimme, *J. Comput. Chem.*, 2006, **27**, 1787-1799.
31. J. R. Chang and S. L. Chang, *J. Catal.*, 1998, **176**, 42-51.
32. J. H. Pazmino, C. S. Bai, J. T. Miller, F. H. Ribeiro and W. N. Delgass, *Catal. Lett.*, 2013, **143**, 1098-1107.
33. B. E. Conway and B. V. Tilak, *Electrochim. Acta.*, 2002, **47**, 3571-3594.
34. D. Merki, H. Vrubel, L. Rovelli, S. Fierro and X. L. Hu, *Chem. Sci.*, 2012, **3**, 2515-2525.
35. J. O. M. Bockris and E. C. Potter, *J. Electrochem. Soc.*, 1952, **99**, 169-186.
36. C. Tsai, F. Abild-Pedersen and J. K. Nørskov, *Nano Lett.*, 2014, **14**, 1381-1387.
37. J. K. Nørskov, T. Bligaard, A. Logadottir, J. R. Kitchin, J. G. Chen, S. Pandelov and J. K. Nørskov, *J. Electrochem. Soc.*, 2005, **152**, J23-J26.
38. J. Greeley, T. F. Jaramillo, J. Bonde, I. B. Chorkendorff and J. K. Nørskov, *Nat. Mater.*, 2006, **5**, 909-913.
39. W. C. Sheng, M. Myint, J. G. G. Chen and Y. S. Yan, *Energy Environ. Sci.*, 2013, **6**, 1509-1512.